

Comparative study of charge order in undoped infinite-layer nickelate superconductors

Yang Shen,¹ Mingpu Qin,^{1,*} and Guang-Ming Zhang^{2,3,†}

¹*Key Laboratory of Artificial Structures and Quantum Control, School of Physics and Astronomy, Shanghai Jiao Tong University, Shanghai 200240, China*

²*State Key Laboratory of Low-Dimensional Quantum Physics and*

Department of Physics, Tsinghua University, Beijing 100084, China

³*Frontier Science Center for Quantum Information, Beijing 100084, China*

To understand the microscopic mechanism of the charge order observed in the parent compound of the infinite-layer nickelate superconductors, we consider a minimal three-legged model consisting of a two-legged Hubbard ladder for the Ni $3d_{x^2-y^2}$ electrons and a free conduction electron chain from the rare-earths. With highly accurate density matrix renormalization group calculations, when the chemical potential difference is adjusted to make the Hubbard ladder with 1/3 hole doping, we find a long-range charge order with period 3 in the ground state of the model, while the spin excitation has a small energy gap. Moreover, the electron pair-pair correlation has a quasi-long-range behavior, indicating an instability of superconductivity even at half-filling. As a comparison, the same method is applied to a pure two-legged Hubbard model with 1/3 hole doping in which the period-3 charge order is a quasi-long range one. The difference between them demonstrates that the free electron chain of the three-legged ladder plays the role of a charge reservoir and enhances the charge order in the undoped infinite-layer nickelates.

I. INTRODUCTION

Since 2019, the family of infinite-layer nickelate superconductors has been synthesized[1–7] which provides another useful platform for the exploration of the microscopic mechanism of unconventional superconductivity. Similar to the cuprates, the infinite-layer nickelates with nominal $3d^9 Ni^+$ contain $3d_{x^2-y^2}$ orbital degree of freedom on a quasi-two-dimensional Ni-O square lattice near the half-filling[8, 9]. However, due to the much larger $p-d$ energy splitting, their low-energy electronic structures are more likely to fall into the Mott-Hubbard than the charge-transfer regime in the Zaanen-Sawatzky-Allen classification scheme[10, 11]. Different from an antiferromagnetic Mott insulator, the resistivity of the parent compounds exhibits metallic behavior at high temperatures and an upturn at low temperatures[1, 12]. No static long-range magnetic order are observed down to the lowest measured temperature[13] though spin fluctuations are reported in experiments[14].

Very recently, a vertical charge order (CO) with period 3 was reported in the undoped parent compound of the infinite-layer nickelates[15–17]. The vertical CO is along the direction of Ni-O bond, different from the diagonal stripe order found in other nickelates[18] where superconductivity is absent. The CO becomes weaker with the increase of doping and finally disappears at 20% doping where superconductivity sets in. Moreover, the X-ray absorption spectroscopy experiments have shown that the doped holes are mainly localized in the Ni $3d_{x^2-y^2}$ orbital, playing the dominant role in the low-energy physics[19]. So it is highly desirable to under-

stand the nature of the undoped parent compound of nickelates.

The existence of competing or intertwining orders is common in cuprates[20]. The CO was observed in many families of cuprates with or without accompanying spin order[21]. Theoretically, the Hubbard model[22–24] is believed to contain the microscopic ingredients of unconventional superconductivity, endowed with a multitude of competing ground-state orders[25]. Though recent result indicates extra terms are needed to account for the superconductivity in the pure [26] two-dimensional Hubbard model [27], vertical stripe order is indeed established in its ground state[28]. In a recent work, the instability of the CO in nickelates was studied in the DFT+DMFT perspective [29]. In this work, to explore the microscopic origin of the CO observed in the undoped parent compound of nickelates, we study a minimal model (we name it nickelate model in this work) in which a two-legged Hubbard ladder describes the Ni $3d_{x^2-y^2}$ electrons and a free electron chain denotes the conduction electrons from the rare-earth ions. As a comparison, we also study a pure [30] two-legged Hubbard ladder with hole doping. These two models are depicted in Fig. 1.

In this work, we employ the density matrix renormalization group (DMRG) method[31, 32], which can provide highly accurate results for the ground state of the nickelate model. When the doping level in the Hubbard chains is tuned to 1/3, a long-range CO with period 3 is found in the Hubbard chains of the three-legged nickelate model. The electron pair-pair correlation decays algebraically with the distance between two pairs. The spin density shows an exponentially decay but has an extremely large correlation length, *i.e.*, larger than 20 lattice constants. We also calculate the pure two-legged Hubbard ladder with 1/3 hole doping, in which a quasi-long range CO is present instead. The comparison indicates the self-doping effect can further enhance

*qinmingpu@sjtu.edu.cn

†gmzhang@tsinghua.edu.cn

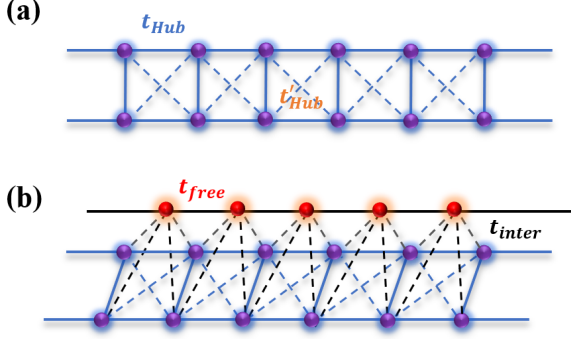


FIG. 1: Schematic illustration of the (a) two-legged Hubbard model and (b) three-legged nickelate model.

the CO, and the Mott-Hubbard type model is relevant to the nickelate superconductors. Similar numerical investigation was carried out for a two-band model on four-legged cylinder[33] which focused on the much smaller self-doping region. We also perform calculation on wider systems and find similar CO near 1/3 self doping but the spin correlation changes to a perfect Neel type in the sense that there is no π -phase spin-flip in the width 4 Hubbard and width 6 nickelate models. The details can be found in the Appendix.

II. MODELS AND METHOD

The nickelate model we consider is a three-legged model with the Hamiltonian

$$\begin{aligned} \hat{H} = & - \sum_{i,j \in H, \sigma} t_{ij} \left(\hat{d}_{i\sigma}^\dagger \hat{d}_{j\sigma} + h.c. \right) + U \sum_{i \in H} \hat{n}_{i\uparrow} \hat{n}_{i\downarrow} \\ & - \sum_{i \in H, k \in F, \sigma} t_{ik} \left(\hat{d}_{i\sigma}^\dagger \hat{c}_{k\sigma} + h.c. \right) - \mu_H \sum_{i \in H} \hat{n}_i, \quad (1) \\ & - \sum_{k,l \in F, \sigma} t_{kl} \left(\hat{c}_{k\sigma}^\dagger \hat{c}_{l\sigma} + h.c. \right) - \mu_F \sum_{k \in F} \hat{n}_k \end{aligned}$$

where $\hat{d}_{i\sigma}^\dagger$ ($\hat{c}_{i\sigma}^\dagger$) is the Ni $3d_{x^2-y^2}$ ($5d$ conduction) electron creation operator on site $i = (x_i, y_i)$ with spin σ , $\hat{n}_i = \sum_{\sigma} \hat{c}_{i\sigma}^\dagger \hat{c}_{i\sigma}$ is the electron number operator, μ_H and μ_F are two chemical potentials, and H and F represent the Hubbard and free chain, respectively. The nearest neighboring hopping amplitude on the Hubbard chains is set as the energy unit, the next nearest neighboring hopping is chosen as $t'_{Hub} = 0.1$, and the on-site Hubbard interaction is set to $U = 12$. The nearest neighboring hopping on the free chain is set to $t_{free} = 1.1$, and the hopping amplitude between the Hubbard and free chains is chosen as $t_{inter} = 0.2$. These chosen parameters are relevant to the experimental materials.

In our study, we assume that the whole system is kept at half-filling, $n = N_e/N_{site} = 1$, and we tune $\delta\mu = \mu_F - \mu_H$ to target the desired hole (electron) doping level on the Hubbard (free) chain. The average of

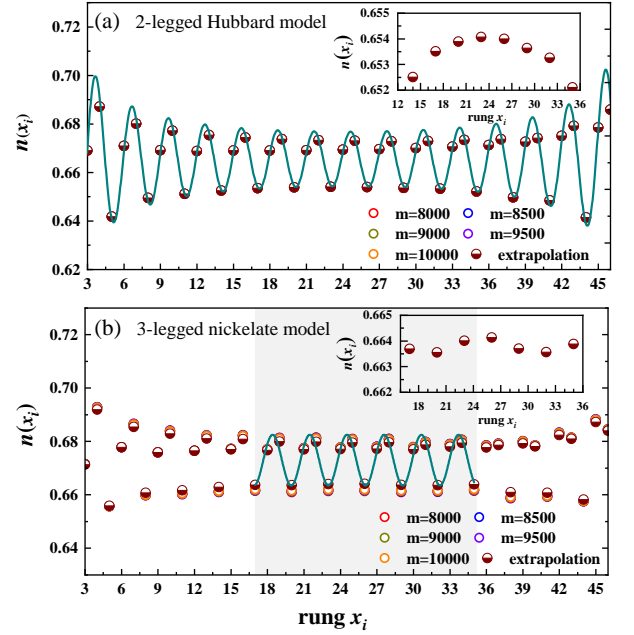


FIG. 2: Charge density profiles at 1/3 hole doping for the (a) two-legged Hubbard model and (b) three-legged nickelate model. The open circles denote the local rung density for different number of kept states m in DMRG calculations and the half-filled one denote the extrapolated values. The solid cyan line in (a) is the fitting curve using Eq. (3). Fitting the results in (b) with Eq. (3) gives both positive and negative K_ρ depending on the range of data used, which indicates it actually oscillates periodically without decay (the cyan line in (b) shows a fit of the results using a cosine function in the middle of the system). The insets show the lower peaks near the center of the systems.

hole concentration away from half-filling for each Hubbard chain is defined as δ , and the corresponding electron doping in the free chain is 2δ . To measure the local spin density $\hat{s}_i = (\hat{n}_{i\uparrow} - \hat{n}_{i\downarrow})/2$ instead of the more demanding spin-spin correlation function, we apply a magnetic pinning field with strength $h_m = 0.5$ at the left edge of one Hubbard chain. We also study the same system without pinning field and find the CO is unchanged in the bulk of the system. The details of the results can be found in the Appendix. We also calculate the pair-pair correlation function $D(i, j) = \langle \hat{\Delta}_i^\dagger \hat{\Delta}_j \rangle$, where

$$\hat{\Delta}_i^\dagger = \hat{c}_{(i,1),\uparrow}^\dagger \hat{c}_{(i,2),\downarrow}^\dagger - \hat{c}_{(i,1),\downarrow}^\dagger \hat{c}_{(i,2),\uparrow}^\dagger, \quad (2)$$

which creates a singlet pair across the rung of the Hubbard ladder.

The method we employ is the DMRG [31, 32], which can provide accurate results for such narrow systems with large enough bond dimension. With open boundary conditions, we focus on ladder with length $L_x = 48$ and tune $\delta\mu = 0.9$ to target 1/3 doping on the Hubbard chains, which is relevant to the experimental observation[15–17]. The number of kept states in the DMRG calculations is as large as $m = 10,000$, which gives truncation errors of

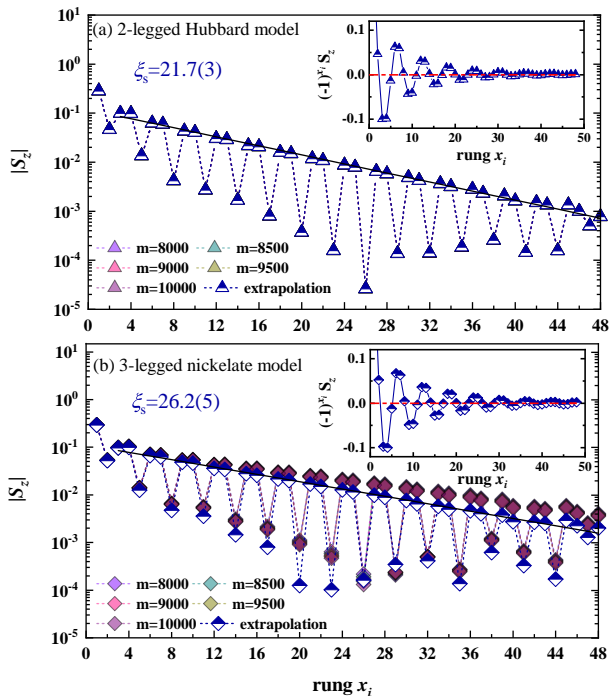


FIG. 3: Absolute values of the spin density on the (a) two-legged Hubbard model and (b) three-legged nickelate model. Both results with finite kept states m (solid markers) and from an extrapolation with truncation errors (half-solid markers) are shown. The insets display the staggered spin density, where the dash-dotted horizontal lines represent zero.

6.90×10^{-9} and 8.92×10^{-6} for the two-legged Hubbard and three-legged nickelate models. For the pure two-legged Hubbard model, the results are converged with kept state, while for the three-legged nickelate model, the free electron chain makes the entanglement larger in the ground state and an extrapolation with truncation errors is also performed to remove the finite kept state effect.

III. NUMERICAL RESULTS

A. Hubbard ladders

In Fig. 2(a), we show the charge density profiles for the two-legged ladder with $\delta = 1/3$. The rung density is defined by $n(x_i) = \sum_{y=1}^{L_y} \langle \hat{n}_i(x, y) \rangle / L_y$ on the Hubbard ladders. The charge density from DMRG with kept states $m = 8000$ to $m = 10000$ and the result from an extrapolation with truncation error are on top of each other, which means the DMRG results in Fig. 2 (a) are converged (the same is true for all the other quantities discussed in the remaining of this work). The charge distribution displays a $\lambda_\rho = 1/\delta$ periodic structure. The vertical CO at long distances is dominated by a power-law decay with the Luttinger exponent K_ρ , which can be fitted by the

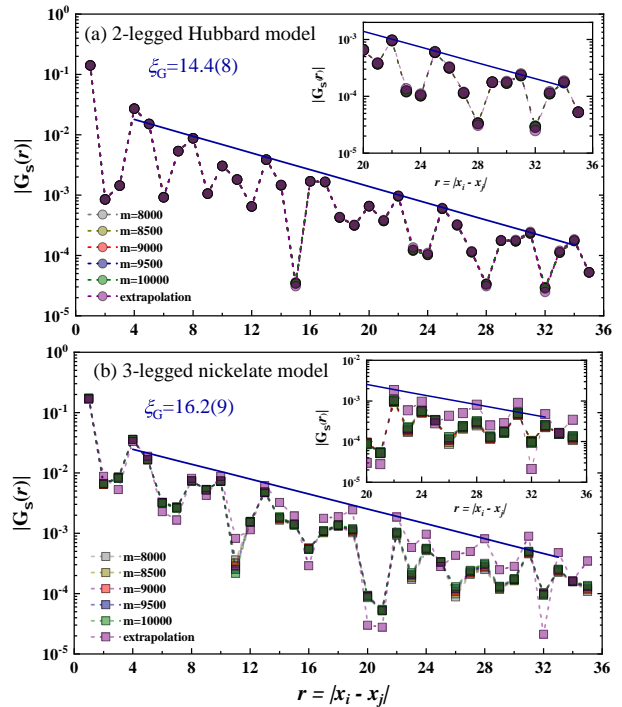


FIG. 4: Single-particle Green's function on the (a) two-legged Hubbard model and (b) three-legged nickelate model. In the calculation of $G_\sigma(r)$, we choose the 13th site on one Hubbard chain as the reference. Both numerical results for finite kept states m and extrapolated results are shown. In the insets, the long-distance behavior is zoomed in.

Friedel oscillations induced by the boundaries[34]

$$n(x) \approx A \frac{\cos(2\pi N_h x/L + \phi_1)}{[L \sin(\pi x/L + \phi_2)]^{K_\rho/2}} + n_0, \quad (3)$$

where A is the amplitude, ϕ_1 and ϕ_2 are phase shifts, and $n_0 = 1 - \delta$ is the mean charge density. Alternatively, we can obtain the parameter K_ρ from the finite-size scaling [35], because the density scales as

$$\delta n(L/2) = n(L/2) - n_0 \sim L^{-K_\rho/2}, \quad (4)$$

around the center of the system. All fitting procedures give the similar values of exponent K_ρ , which is close to 1.21(6). The details of the fittings can be found in the Appendix.

The rung density $n(x)$ on the three-legged nickelate model from DMRG with $m = 8000$ to $m = 10000$ are shown in Fig. 2 (b). Since the three-legged system has a larger truncation error than the two-legged Hubbard model in the DMRG calculation, we also perform an extrapolation with truncation error ϵ to remove the finite kept state effect.

A fit following the same procedure as in the two-legged Hubbard model for the CO correlation on the three-legged nickelate model gives both positive and negative K_ρ depending on the range of data used, which indicates it actually oscillates periodically without decay, or

$K_\rho \approx 0$, suggesting the CO is actually a long-range one in the three-legged nickelate model. The details can be found in the Appendix.

The insets in Fig. 2 show the lower peaks near the center of the systems. In the inset of Fig. 2 (a), we find a decay from the center behavior which shows the envelope of the oscillation of density governed by Eq. (3), while in the inset of Fig. 2 (b), we find that the lower peak of density oscillates without decay near the center which is the hallmark of the existence of true long-range CO in the nickelate model. Comparing the CO in the three-legged nickelate model and the pure two-legged Hubbard model, we conclude that the free electron chain, which plays the role of a charge reservoir, can enhance the CO in the nickelate model. We also observe an induced CO in the free chain with period 6 in the nickelate model as will be shown later.

In Fig. 3, we display the absolute value of magnetization $\langle \hat{s}_i^z \rangle$ with different number of kept states m in DMRG calculations as well as the extrapolated result. For both systems, $\langle \hat{s}_i^z \rangle$ displays an exponential decay as $\langle \hat{s}_i^z \rangle \propto e^{-x_i/\xi_s}$ at long distances, with a finite correlation length ξ_s . Comparing with the two-legged Hubbard model, the three-legged nickelate model has a slightly larger ξ_s , implying a smaller spin excitation gap. The staggered spin density $(-1)^{x_i} \langle \hat{s}_i^z \rangle$ in the insets of Fig. 3 show a spatial modulation with a wavelength twice that of the charge density, and have a π phase flip at the hole-concentrated sites, which is the feature of the so-called stripe order[36–39].

The single-particle Green's function of the electrons on the Hubbard ladder is defined by

$$G_\sigma(r) = \langle \hat{c}_{(x_0,y),\sigma}^\dagger \hat{c}_{(x_0+r,y),\sigma} \rangle, \quad (5)$$

which involves both charge and spin degrees of freedom. The corresponding numerical result has shown in Fig. 4. Due to the presence of the small energy gap in the spin excitations, this electron Green's function is found decaying exponentially as $G_\sigma(r) \propto e^{-r/\xi_G}$, from which a correlation length can be extracted as $\xi_G = 14.4(8)$ and $16.2(9)$ for the two-legged Hubbard model and three-legged nickelate model, respectively.

More importantly, the singlet pair-pair correlation function $D(i, j)$ for the pure two-legged Hubbard model and the three-legged nickelate model are also calculated and displayed in Fig. 5. The given numerical results are from the extrapolation with truncation error in DMRG calculations. The details of extrapolation are provided in the Appendix. The singlet pair-pair correlation function decays algebraically for both systems, *i.e.*, $D(r) \propto r^{-K_{sc}}$ with $K_{sc}=1.3(1)$ and $K_{sc} = 1.2(1)$ for the pure two-legged Hubbard model and the three-legged nickelate model, respectively. The algebraic decay of pairing correlation indicates the instability of superconductivity in both systems.

Finally we summarize the exponents and correlation lengths for the charge, spin, single-particle, and singlet pairing of the correlation functions for both models with

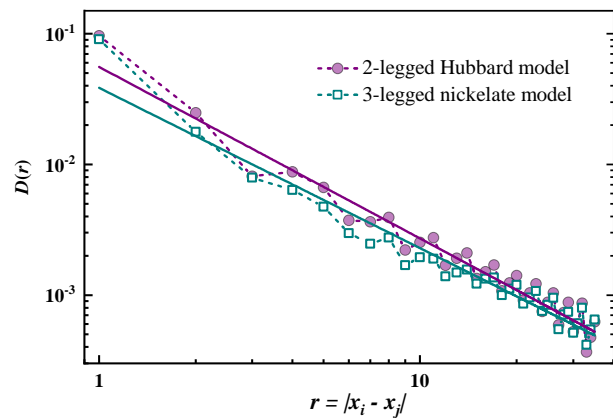


FIG. 5: Pair-pair correlation function for the two-legged Hubbard model (solid circle) and three-legged nickelate model (empty square) at 1/3 doping. In the calculation of $D(r)$, we choose the 13th vertical bond as the reference. The power-law fits $D(r) \propto r^{-K_{sc}}$ for both systems give close exponents K_{sc} . Only extrapolated results with truncation errors are shown. Results with finite kept state and the extrapolation can be found in the Appendix.

TABLE I: List of the extracted parameters for charge, spin, pair-pair correlations, and single-particle Green's function. Both the two-legged Hubbard model and the three-legged nickelate model results are shown for comparison.

	hole	K_ρ	K_{sc}	ξ_s	ξ_G
2-legged Hubbard model	1/3	1.21(6)	1.3(1)	21.7(3)	14.4(8)
3-legged nickelate model	0.3255	0	1.2(1)	26.2(5)	16.2(9)

1/3 hole doping in Table. I. Comparing the three-legged nickelate and the two-legged Hubbard model, the major difference is the enhancement of charge order by including the charge reservoir, while the pairing, spin, and single particle properties are very similar. Therefore, within the simplified model Hamiltonian, the present numerical results have clearly demonstrated their similarities between the nickelates and cuprates.

B. Free chain in the three-legged nickelate model

In Fig. 6, we show the local charge density, local spin density, single-particle Green's function, and pair-pair correlation for the free chain in the three-legged nickelate model. Because the whole system is set at half-filling and the Hubbard chains of the three-legged nickelate model are about 1/3 hole-doped, the free chain is electron doped (with averaged density about 5/3). We can find an induced charge order with period 6 in the free chain, while the induced spin density is negligibly small due to the absence of the Hubbard interaction. We can also find an induced quasi-long range like pair-pair correlation with the same period as the local charge density.

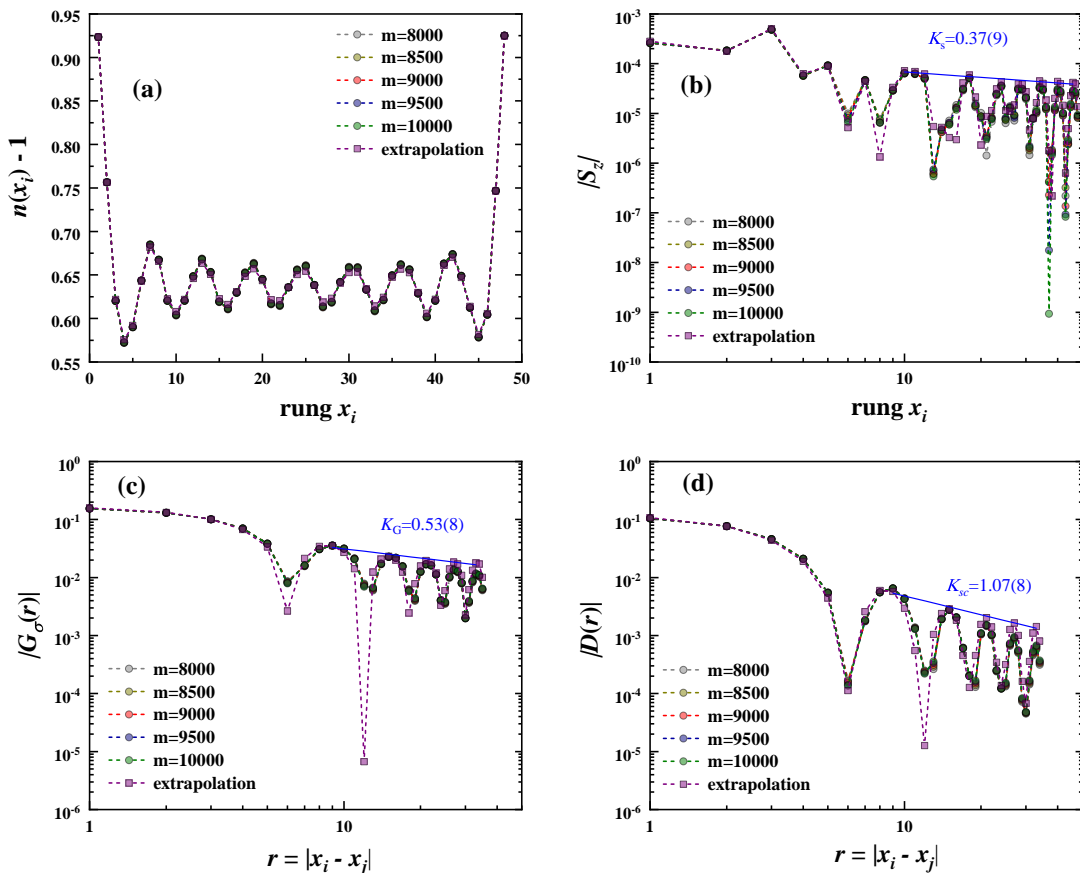


FIG. 6: (a) local charge density, (b) local spin density, (c) single-particle Green's function, and (d) pair-pair correlation on the free chain of the three-legged nickelate model. The reference bond (site) is set at the 13th horizontal bond (site) when calculating $D(r)$ ($G_\sigma(r)$). Solid lines are algebraic fits and the corresponding exponents are listed. The induced charge order in the free chain has a period of 6 lattice constants.

IV. SUMMARY AND PERSPECTIVES

We have studied a three-legged nickelate model which might be relevant to the infinite-layer nickelate superconductors. Our accurate DMRG calculations have yielded a long-range charge order with period 3 in the undoped compound due to the presence of self-doping effect from the rare-earth-layer $5d$ itinerant electrons. Our results are consistent with spectroscopic experiments[16, 17], which showed a charge order resulted from the strong correlation of Ni $3d$ orbitals and self-doping effect from the Nd $5d$ orbitals. Remarkably, different from the quasi-long range charge order in the pure two-legged Hubbard with $1/3$ hole doping, the charge order in three-legged nickelate model is long-ranged instead, indicating that the charge reservoir of the free chain can enhance the charge order in the Hubbard ladder. At the same time, a small energy gap is present in the spin excitations, leading to an extremely large correlation length.

A quasi-long-range pairing correlation is also determined in the nickelate model, which might be a precursor of superconducting order in two dimension case with tuned parameters. Although we focus on the par-

ent compound in this work, it is usually believed that the long-range charge order disfavors the superconductivity. Experimentally, the charge order becomes weaker with the increase of hole doping and finally disappears at 20% hole doping, where the superconductivity sets in[16]. How the charge order melts with hole doping in the nickelate model and the evolution of pairing correlation with doping will be an interesting topic for future study.

V. ACKNOWLEDGMENTS

Y. Shen and M. P. Qin thank Weidong Luo for his generosity to provide computational resources for this work. G. M. Zhang acknowledges the support from the National Key Research and Development Program of MOST of China (2017YFA0302902). M. P. Qin acknowledges the support from the National Key Research and Development Program of MOST of China (2022YFA1405400), the National Natural Science Foundation of China (Grant No. 12274290) and the sponsorship from Yangyang Development Fund. All the DMRG calculations are carried out with iTensor library [40].

- [1] D. Li, K. Lee, B. Y. Wang, M. Osada, S. Crossley, H. R. Lee, Y. Cui, Y. Hikita, and H. Y. Hwang, *Nature* **572**, 624 (2019).
- [2] Y. Nomura and R. Arita, *Reports on Progress in Physics* (2022).
- [3] D. Li, B. Y. Wang, K. Lee, S. P. Harvey, M. Osada, B. H. Goodge, L. F. Kourkoutis, and H. Y. Hwang, *Phys. Rev. Lett.* **125**, 027001 (2020), URL <https://link.aps.org/doi/10.1103/PhysRevLett.125.027001>.
- [4] S. Zeng, C. S. Tang, X. Yin, C. Li, M. Li, Z. Huang, J. Hu, W. Liu, G. J. Omar, H. Jani, et al., *Phys. Rev. Lett.* **125**, 147003 (2020), URL <https://link.aps.org/doi/10.1103/PhysRevLett.125.147003>.
- [5] M. Osada, B. Y. Wang, K. Lee, D. Li, and H. Y. Hwang, *Phys. Rev. Materials* **4**, 121801 (2020), URL <https://link.aps.org/doi/10.1103/PhysRevMaterials.4.121801>.
- [6] M. Osada, B. Y. Wang, B. H. Goodge, S. P. Harvey, K. Lee, D. Li, L. F. Kourkoutis, and H. Y. Hwang, *Advanced Materials* **33**, 2104083 (2021), URL <https://onlinelibrary.wiley.com/doi/abs/10.1002/adma.202104083>.
- [7] S. Zeng, C. Li, L. E. Chow, Y. Cao, Z. Zhang, C. S. Tang, X. Yin, Z. S. Lim, J. Hu, P. Yang, et al., *Science Advances* **8**, eabl9927 (2022), <https://www.science.org/doi/pdf/10.1126/sciadv.abl9927>, URL <https://www.science.org/doi/abs/10.1126/sciadv.abl9927>.
- [8] V. Anisimov, D. Bukhvalov, and T. Rice, *Physical Review B* **59**, 7901 (1999).
- [9] K.-W. Lee and W. Pickett, *Physical Review B* **70**, 165109 (2004).
- [10] J. Zaanen, G. A. Sawatzky, and J. W. Allen, *Phys. Rev. Lett.* **55**, 418 (1985), URL <https://link.aps.org/doi/10.1103/PhysRevLett.55.418>.
- [11] B. H. Goodge, D. Li, K. Lee, M. Osada, B. Y. Wang, G. A. Sawatzky, H. Y. Hwang, and L. F. Kourkoutis, *Proceedings of the National Academy of Sciences* **118**, e2007683118 (2021), <https://www.pnas.org/doi/pdf/10.1073/pnas.2007683118>, URL <https://www.pnas.org/doi/abs/10.1073/pnas.2007683118>.
- [12] G.-M. Zhang, Y.-F. Yang, and F.-C. Zhang, *Phys. Rev. B* **101**, 020501 (2020), URL <https://link.aps.org/doi/10.1103/PhysRevB.101.020501>.
- [13] M. Hayward and M. Rosseinsky, *Solid State Sciences* **5**, 839 (2003), ISSN 1293-2558, international Conference on Inorganic Materials 2002, URL <https://www.sciencedirect.com/science/article/pii/S1293255803001110>.
- [14] H. Lu, M. Rossi, A. Nag, M. Osada, D. F. Li, K. Lee, B. Y. Wang, M. Garcia-Fernandez, S. Agrestini, Z. X. Shen, et al., *Science* **373**, 213 (2021), <https://www.science.org/doi/pdf/10.1126/science.abd7726>, URL <https://www.science.org/doi/abs/10.1126/science.abd7726>.
- [15] M. Rossi, M. Osada, J. Choi, S. Agrestini, D. Jost, Y. Lee, H. Lu, B. Y. Wang, K. Lee, A. Nag, et al., arXiv preprint arXiv:2112.02484 (2021).
- [16] G. Krieger, L. Martinelli, S. Zeng, L. Chow, K. Kummer, R. Arpaia, M. M. Sala, N. Brookes, A. Ariando, N. Viart, et al., arXiv preprint arXiv:2112.03341 (2021).
- [17] C. C. Tam, J. Choi, X. Ding, S. Agrestini, A. Nag, B. Huang, H. Luo, M. García-Fernández, L. Qiao, and K.-J. Zhou, arXiv preprint arXiv:2112.04440 (2021).
- [18] J. M. Tranquada, D. J. Buttrey, V. Sachan, and J. E. Lorenzo, *Phys. Rev. Lett.* **73**, 1003 (1994), URL <https://link.aps.org/doi/10.1103/PhysRevLett.73.1003>.
- [19] M. Rossi, H. Lu, A. Nag, D. Li, M. Osada, K. Lee, B. Y. Wang, S. Agrestini, M. Garcia-Fernandez, J. J. Kas, et al., *Phys. Rev. B* **104**, L220505 (2021), URL <https://link.aps.org/doi/10.1103/PhysRevB.104.L220505>.
- [20] E. Fradkin, S. A. Kivelson, and J. M. Tranquada, *Rev. Mod. Phys.* **87**, 457 (2015), URL <https://link.aps.org/doi/10.1103/RevModPhys.87.457>.
- [21] J. M. Tranquada, *Advances in Physics* **69**, 437 (2020), <https://doi.org/10.1080/00018732.2021.1935698>, URL <https://doi.org/10.1080/00018732.2021.1935698>.
- [22] J. Hubbard, *Proceedings of the Royal Society of London A: Mathematical, Physical and Engineering Sciences* **276**, 238 (1963), ISSN 0080-4630, URL <http://rspa.royalsocietypublishing.org/content/276/1365/238>.
- [23] M. Qin, T. Schäfer, S. Andergassen, P. Corboz, and E. Gull, *Annual Review of Condensed Matter Physics* **13**, 275 (2022), <https://doi.org/10.1146/annurev-conmatphys-090921-033948>, URL <https://doi.org/10.1146/annurev-conmatphys-090921-033948>.
- [24] D. P. Arovas, E. Berg, S. A. Kivelson, and S. Raghu, *Annual Review of Condensed Matter Physics* **13**, 239 (2022), <https://doi.org/10.1146/annurev-conmatphys-031620-102024>, URL <https://doi.org/10.1146/annurev-conmatphys-031620-102024>.
- [25] D. J. Scalapino, *Rev. Mod. Phys.* **84**, 1383 (2012), URL <https://link.aps.org/doi/10.1103/RevModPhys.84.1383>.
- [26] Pure means only nearest neighbouring hoppings are considered in the Hubbard model.
- [27] M. Qin, C.-M. Chung, H. Shi, E. Vitali, C. Hubig, U. Schollwöck, S. R. White, and S. Zhang (Simons Collaboration on the Many-Electron Problem), *Phys. Rev. X* **10**, 031016 (2020), URL <https://link.aps.org/doi/10.1103/PhysRevX.10.031016>.
- [28] B.-X. Zheng, C.-M. Chung, P. Corboz, G. Ehlers, M.-P. Qin, R. M. Noack, H. Shi, S. R. White, S. Zhang, and G. K.-L. Chan, *Science* **358**, 1155 (2017), <https://www.science.org/doi/pdf/10.1126/science.aam7127>, URL <https://www.science.org/doi/abs/10.1126/science.aam7127>.
- [29] K. G. Slobodchikov and I. V. Leonov, arXiv e-prints arXiv:2206.06985 (2022), 2206.06985.
- [30] Pure here means the free electron chain in the three-legged nickelate model is removed.
- [31] S. R. White, *Phys. Rev. Lett.* **69**, 2863 (1992), URL <https://link.aps.org/doi/10.1103/PhysRevLett.69.2863>.
- [32] S. R. White, *Phys. Rev. B* **48**, 10345 (1993), URL <https://link.aps.org/doi/10.1103/PhysRevB.48.10345>.
- [33] C. Peng, H.-C. Jiang, B. Moritz, T. P. Devereaux, and C. Jia, arXiv e-prints arXiv:2110.07593 (2021), 2110.07593.
- [34] S. R. White, I. Affleck, and D. J. Scalapino, *Phys. Rev. B* **65**, 165122 (2002), URL <https://link.aps.org/doi/10.1103/PhysRevB.65.165122>.

- 10.1103/PhysRevB.65.165122.
- [35] M. Dolfi, B. Bauer, S. Keller, and M. Troyer, Phys. Rev. B **92**, 195139 (2015), URL <https://link.aps.org/doi/10.1103/PhysRevB.92.195139>.
- [36] J. Zaanen and O. Gunnarsson, Phys. Rev. B **40**, 7391 (1989), URL <https://link.aps.org/doi/10.1103/PhysRevB.40.7391>.
- [37] M. Kato, K. Machida, H. Nakanishi, and M. Fujita, Journal of the Physical Society of Japan **59**, 1047 (1990), <https://doi.org/10.1143/JPSJ.59.1047>, URL <https://doi.org/10.1143/JPSJ.59.1047>.
- [38] D. Poilblanc and T. M. Rice, Phys. Rev. B **39**, 9749 (1989), URL <https://link.aps.org/doi/10.1103/PhysRevB.39.9749>.
- [39] Schulz, H.J., J. Phys. France **50**, 2833 (1989), URL <https://doi.org/10.1051/jphys:0198900500180283300>.
- [40] M. Fishman, S. R. White, and E. Miles Stoudenmire, arXiv e-prints arXiv:2007.14822 (2020), 2007.14822.

Appendix A: Dependence of K_ρ on the range of data

In Table. II, we list the extracted K_ρ and n_0 using Eq. (3) in the main text for the two-legged 1/3 hole doped Hubbard model with length $L = 48$. The values of K_ρ are obtained from the fits by using charge density from different range of sites. The results are consistent with the values in the main text $K_\rho = 1.21(6)$.

In Fig. 7, we show the fit using the value at the center of the systems for different sizes following Eq. (4) in the main text. The extracted K_ρ is consistent with the values listed in Table. II.

In Table. III, we list the extracted K_ρ and n_0 using Eq. (3) in the main text for the three-legged 1/3 hole doped nickelate model with length $L = 48$. The values of K_ρ are obtained from the fits by using charge density from different range of sites. We can find that the fit gives that both positive and negative K_ρ depending on the range of data used, which indicates it actually oscillates periodically without decay, or $K_\rho \approx 0$, suggesting the CO is actually a long-range one in the three-legged nickelate model.

TABLE II: The dependence of the extracted K_ρ and n_0 (using Eq. (3) in the main text) on the range of sites used in the fit for the two-legged Hubbard model ($L = 48$).

range of sites	K_ρ	n_0	R^2
#03 ~ #(L-2)	1.23(3)	0.66552(6)	0.99665
#06 ~ #(L-5)	1.20(5)	0.66561(6)	0.99754
#09 ~ #(L-8)	1.17(4)	0.66544(3)	0.99960
#12 ~ #(L-11)	1.11(4)	0.66549(2)	0.99990
#15 ~ #(L-14)	1.13(7)	0.66552(2)	0.99993

TABLE III: The dependence of the extracted K_ρ and n_0 (using Eq. (3) in the main text) on the range of sites used in the fit for the three-legged nickelate model ($L = 48$).

range of sites	K_ρ	n_0	R^2
#03 ~ #(L-2)	-0.2(6)	0.6718(9)	0.5461
#06 ~ #(L-5)	0(1)	0.6722(7)	0.6923
#09 ~ #(L-8)	1(1)	0.6725(6)	0.7864
#12 ~ #(L-11)	0.1(3)	0.6729(5)	0.8681
#15 ~ #(L-14)	0.1(3)	0.6731(5)	0.9123

Appendix B: Extrapolation with truncation errors in DMRG

In Fig. 8, we show the extrapolation of DMRG results for local charge density, the single-particle Green's function, pair-pair correlation, and local spin density with truncation errors. We choose three typical sites in Fig. 8. The local quantities (charge and spin) are extrapolated with truncation error, while the correlations (single-particle Green's function and pair-pair correlation) are extrapolated with the square root of the truncation error.

Appendix C: Results without magnetic pinning field

We also perform calculation of the three-legged nickelate model without any magnetic pinning field. In the left panel of Fig. 9 we show how the local spin density vanishes with the the increase of bond dimension m . The local spin density is under 10^{-6} with bond dimension $m = 9000$ which means the SU(2) symmetry is almost

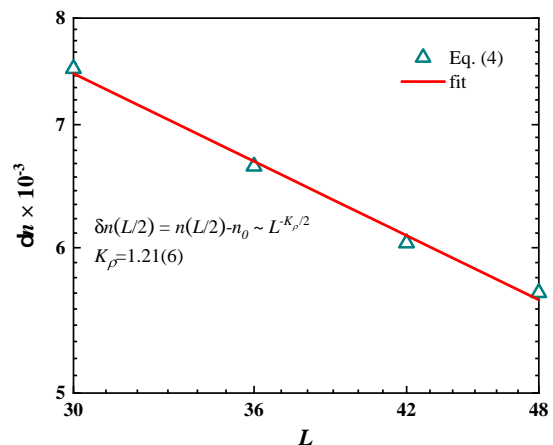


FIG. 7: Finite-size scaling of $\delta n(L/2)$ as a function of the system size L for the two-legged Hubbard model.

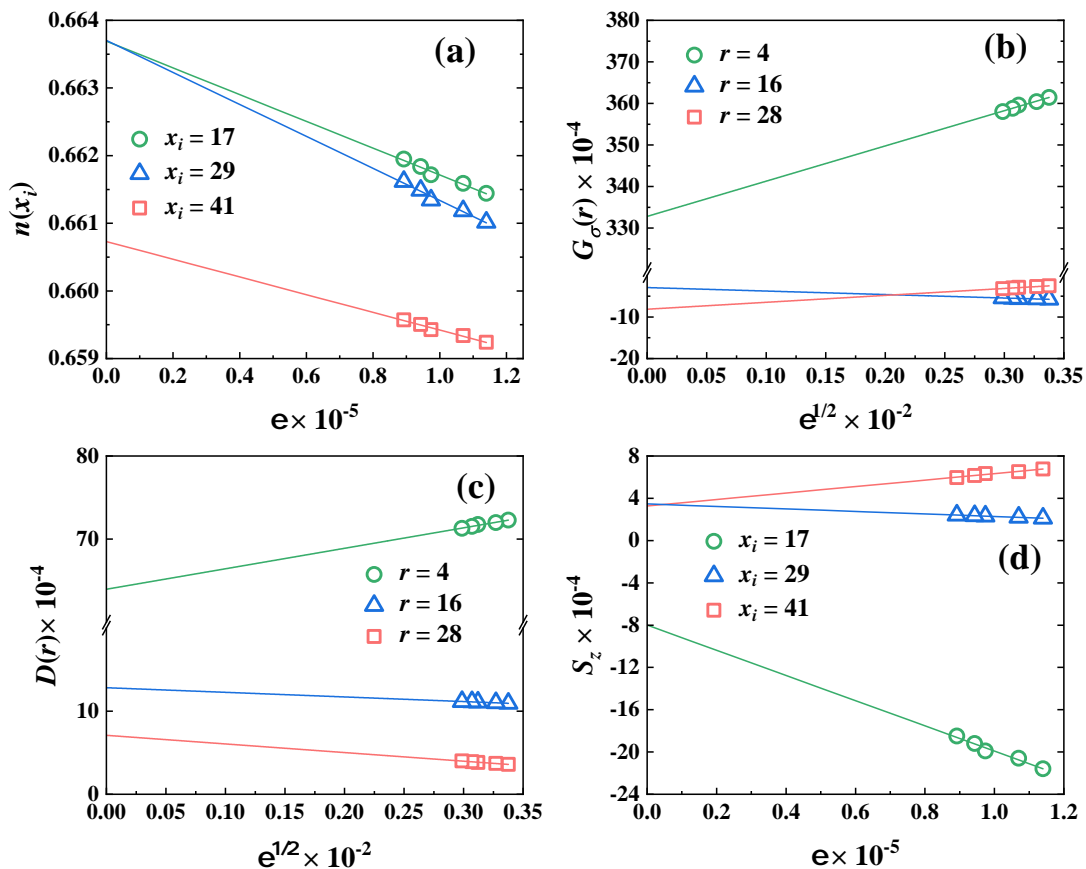


FIG. 8: Extrapolation of observables of the three-legged nickelate model as a function of the truncated error ϵ in DMRG calculations. Representative examples of (a) the local rung density $n(x_i)$, (b) single-particle Green's function $G_\sigma(r)$, (c) pair-pair correlation function $D(r)$, and (d) local spin $\langle \hat{s}_i^z \rangle$ are shown. The reference bond (site) is set at the 13th vertical bond (site on one Hubbard chain) when calculating $D(r)$ ($G_\sigma(r)$). Local observables such as charge density and spin density are fitted linearly with ϵ , while correlation functions are fitted linearly with $\sqrt{\epsilon}$.

restored and the DMRG results are well converged. In the right panel of Fig. 9 we show a comparison of the charge density with and without pinning field on the left edge. We can find that the charge density remains almost unchanged in the bulk, though the results in the left edge show discrepancy as expected.

Appendix D: Results for width-4 and width-6 systems

We also study the Hubbard and nickelate models on width 4 and 6 ladders. The charge, spin and pairing

correlation are shown in Fig. 10. The period 3 CO is also found in these wider system. But different from the 2-legged Hubbard and 3-legged nickelate models, there is no π phase flip in the spin order which means the spin correlation is perfect Neel type. But we can still find a similar period 6 modulation in the spin density. The result in the right panel of Fig. 10 shows pairing correlation is suppressed in wider system.

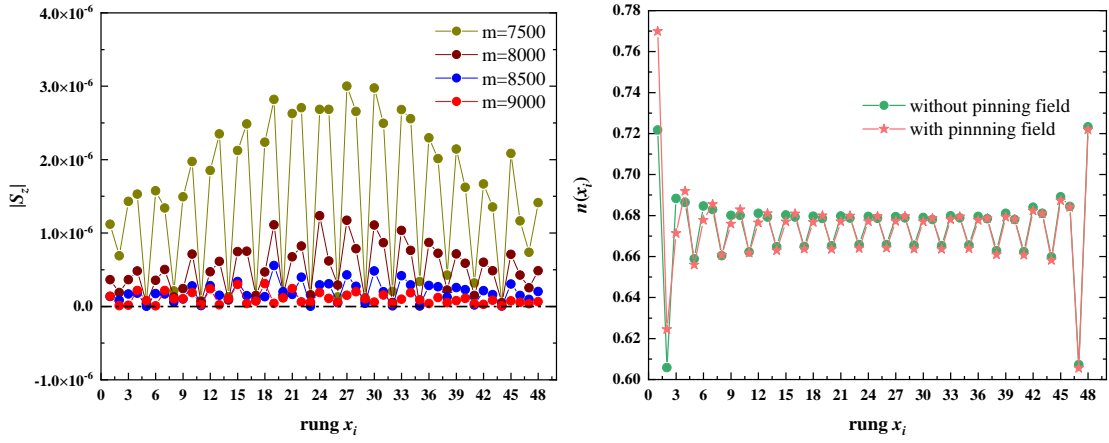


FIG. 9: Left: the vanish of local spin density with the increase of bond dimension m for the three-legged nickelate model without magnetic pinning field. Right: comparison of the charge density for system with and without edge pinning field for the two-legged Hubbard model.

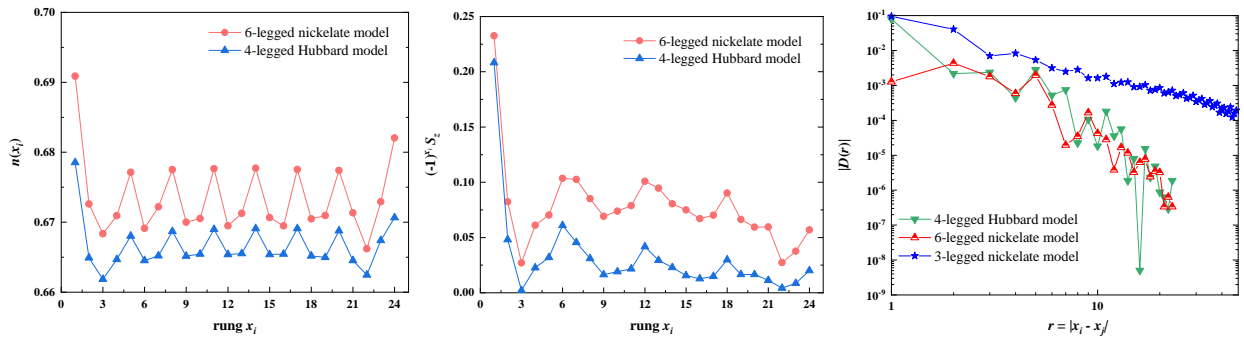


FIG. 10: Charge density (left), spin density (middle), and pair-pair correlation (right) for the 4-legged Hubbard and 6-legged nickelate models. In the left panel, we can find that the period 3 CO remains the same as the 2-legged and 3-legged systems. In the middle panel, the spin changes to Neel antiferromagnetic type without π phase flip found in the 2-legged and 3-legged systems. In the right panel, the pairing is found to be suppressed comparing to 3-legged systems.